LANGMUIR

pubs.acs.org/Langmuir Article

N-Doping Carbon-Nanotube Membrane Electrodes Derived from Covalent Organic Frameworks for Efficient Capacitive Deionization

Li Ren, Jiemei Zhou, Sen Xiong,* and Yong Wang*

Cite This: *Langmuir* 2020, 36, 12030−12037 Read Online

ACCESS | Metrics & More | Article Recommendations | Supporting Information

ABSTRACT: Capacitive deionization (CDI) is an energy-efficient and environmentally friendly electrochemical desalination technology which has attracted increasing attention in recent years. Electrodes are crucial to the performance of CDI processes, and utilizing a carbon-nanotubes (CNTs) membrane to fabricate electrodes is an attractive solution for advanced CDI processes. However, the strong hydrophobicity and low electrosorption capacity limit applications of CNTs membranes in CDI. To solve this problem, we introduce crystalline porous covalent organic frameworks (COFs) into CNTs membranes to fabricate N-doping carbon-nanotubes membrane electrodes (NCMEs). After solvothermal growth and carbonization, CNTs membranes are successfully coated with imine-based COFs and turned into integrated NCMEs. Comparing with the CNTs membranes, the NCMEs exhibit an ∼2.3 times higher electrosorption capacity and superior reusability. This study not only confirms that COFs can be used as high-quality carbon sources but also provides a new strategy to fabricate high-performance CDI electrodes.

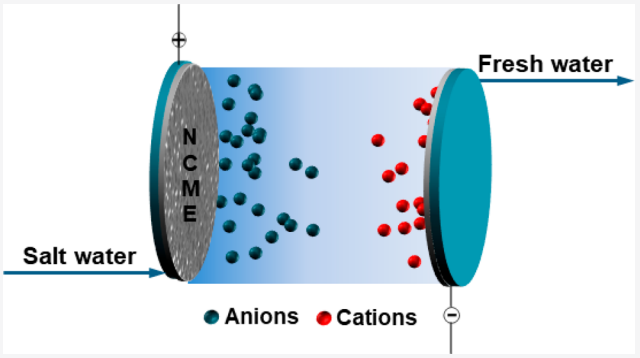

INTRODUCTION

Capacitive deionization (CDI) is a novel water treatment technology that has attracted considerable interest in recent years.[1−4] Through the utilization of an electric field force, the CDI electrodes can adsorb oppositely charged species from solutions. After cutting off or reversing the voltage applied on electrodes, the ions adsorbed on the electrode surface will be released and the electrodes are regenerated. Comparing with other desalination technologies, such as multistage flash (MSF),[5] reverse osmosis (RO),[6] and electrodialysis (ED),[7] CDI features environmental friendliness, high desalination efficiency, and easy scalability.[8,9] Due to these advantages, CDI has been successfully utilized in desalination,[10,11] water softening,[12] heavy metal removal,[13] and wastewater treatment.[14] It is worth noting that the deionization performance of CDI processes is mainly dependent on the properties of the electrodes. Hence, developing high-performance electrodes with desirable conductivity, electrosorption capacity, pore structure, and electrochemical stability will significantly promote the performance of CDI systems.

Due to the easily available raw materials and acceptable conductivity, common carbon-based materials including carbon gel (CA),[15] activated carbon (AC),[16] graphene,[17,18] and carbon-nanotubes (CNTs)[19] are widely used as electrode materials to fabricate CDI electrodes. However, these materials are difficult to meet the desired properties simultaneously, such as good electrical conductivity, high specific surface area, and appropriate pore size distribution. Therefore, some active materials, such as biomass-derived carbons, conductive polymers, and conductive agents are doped into carbon materials to enhance the performance of electrodes.[20−23] Yan et al. fabricated CNTs and AC hybrid electrodes by chemical vapor deposition. Since CNTs provided a robust structure and conductive pathway for AC granules, the highly conductive hybrid electrodes exhibited superior salt adsorption capacity with long-term stability.[23] Zhang et al. reported that metal−organic gels (MOGs)-derived porous carbon could be used as CDI electrodes and exhibited a high salt removal capacity, which was ascribed to its high specific surface area and suitable pore size distribution to facilitate ions to pass.[24]

Research further confirms that introducing the nitrogen (N) element into carbon materials will facilitate the transport of electrons, prevent carbon oxidation, and increase active sites, thereby promoting the CDI performance of electrodes. Hu et al. reported that N-doped AC was used as a positive electrode in asymmetric CDI cells. The doping of N significantly improved the long-term stability of the electrodes.[25] Yamauchi and co-workers attributed the performance promotion of N-

Received: August 14, 2020
Revised: September 21, 2020
Published: September 21, 2020

https://dx.doi.org/10.1021/acs.langmuir.0c02405
Langmuir 2020, 36, 12030−12037

Scheme 1. Schematic Diagram of NCMEs Preparation Processes

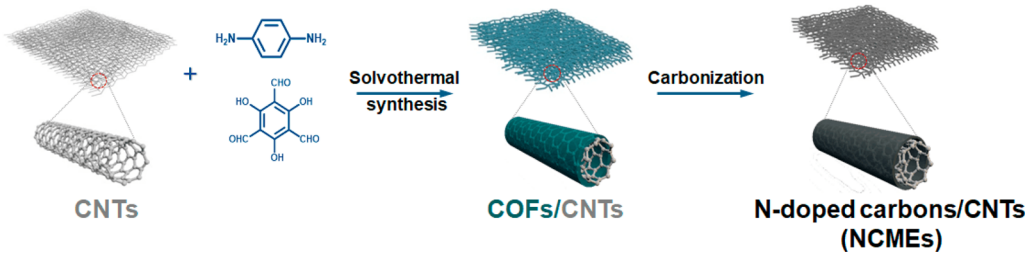

doped electrodes to the atomic level hybridization of the N elements into the chemical structure of the carbon materials. The N element aided formation of five- or six-membered rings, thus forming graphitic, pyridinic, or pyrrolic N structures. The graphitic N structure could facilitate the transfer of electrons; meanwhile, the pyridinic and pyrrolic N structures with rich electrons made it easier to capture cations.[26] These results indicate that both N doping and pore size adjustment are effective methods to improve the performance of electrodes. However, few methods could combine these two methods together.

Nowadays, metal organic frameworks (MOFs) and covalent organic frameworks (COFs) are emerging materials with the merits of a large specific surface area, ordered pore sizes, and good electrochemical stability, which have been applied in energy storage,[27−29] membrane separation,[30,31] semiconductors,[32] and many other fields. Moreover, the abundant organic components in these materials make them excellent precursors to fabricate carbon-based materials. Zhang et al. coated zeolitic imidazolate frameworks (ZIF-8) on polyacrylonitrile (PAN) nanofibers to fabricate N-doped porous CNTs electrodes. Due to the high N concentration and macroporous structure with lateral mesopores, the electrodes exhibited a high salt adsorption capacity and good reusability.[33] Unfortunately, the metal ions in MOFs would hinder the electrosorption processes and should be removed from the carbon materials before being used as electrodes, which makes the fabrication processes of MOFs-based electrodes cumbersome.[33,34]

As the counterparts of MOFs, the metal-free COFs have drawn increasing attention for electrode fabrication. Different from the metal−ligand coordination bonds, the covalent bonds endow COFs with higher charge carrier current and thermal and chemical stabilities. Among all kinds of COFs, the triazine- and imine-based COFs with a high nitrogen content are particularly suitable for electrode fabrication. Zhang et al. fabricated covalent triazine frameworks (*p*-CTFs) by ionothermal synthesis. The obtained *p*-CTFs with a high nitrogen content and abundant micropore structures were applied as membrane-type CDI electrodes, which exhibited outstanding electrosorption capacity and regeneration performance.[35] Except for directly being used as electrodes, a COF synthesized from 1,3,5-triformylphloroglucinol (Tp) and *p*-phenylenediamine (Pa), i.e., TpPa, has been used as a precursor to fabricate N-doped carbon electrodes. Due to the heteroatom effect, porous structure, and large interlayer distance, the N-doped carbon materials derived from TpPa have been used in lithium-ion batteries (LIBs) and sodium-ion batteries (SIBs) as anodes, which exhibited excellent electrochemical performance and long-life cycling stability.[34] However, the majority of COFs or N-doped carbon materials are powders, which require adding conductive additives and binders to form electrodes and take the risk of pore blocking and performance degradation.

To integrate the advantages of the functionalization methods mentioned above, we propose an easy but effective strategy to fabricate high-performance N-doping carbon-nanotubes membrane electrodes (NCMEs). Free-standing CNTs membranes with three-dimensional interconnected porous network structures are promising substrates for CDI processes, which have been confirmed by our previous work.[36] To further improve the CDI performance of CNT-based electrodes, we coated TpPa onto CNTs membranes through solvothermal synthesis and then carbonized the TpPa-coated CNTs membranes to acquire NCMEs. Through this two-step strategy, we integrate N doping, pore size adjustment, and electrode molding into the carbonization step to enable a dramatic reduction of time- and labor-consuming functionalization processes on the one hand and avoid using the functionalized porous carbon materials in powder form on the other. No conductive additives and binders are required during the electrode fabrication procedure, and the agglomeration of carbon materials is also solved; thus, the pores of porous carbon materials are well preserved. The fabricated NCMEs exhibit good desalination performance and reusability, which provides a promising strategy to prepare high-performance electrodes for many other electrochemical applications other than CDI processes.

EXPERIMENTAL SECTION

Materials. The multiwalled CNTs membranes were purchased from Suzhou Jiedi Nanotechnology Co., Ltd. 1,3,5-Triformylphloroglucinol (Tp, 95%) and *p*-phenylenediamine (Pa, 97%) were supplied by TongChuangYuan Pharmaceutical (Sichuan, China) and Aladdin, respectively. 1,4-Dioxane (99.5%), mesitylene (99.5%), and anhydrous acetic acid (99.5%) were purchased from Aladdin. Tetrahydrofuran (99.5%) and acetone (99.5%) were supplied by Sinopharm Chemical Reagent Co., Ltd. Anhydrous ethanol, sodium chloride (99.5%), and deionized water were obtained from local suppliers.

Electrode Preparation and CDI Performance Testing. As shown in Scheme 1, the NCMEs were prepared through solvothermal synthesis and carbonization. Different amounts of Tp (0.2, 1, and 2 mmol) with proportional Pa (mole ratio of Tp to Pa is 1:1.5) were dissolved in 50 mL of 1,4-dioxane and mesitylene mixtures (volume ratio is 1:1) as the mother solution. After forming a homogeneous solution, the mother solution was transferred into a Teflon-lined autoclave. Then 0.5 mL of acetic acid was added as the catalyst, while two CNTs membranes (5 × 5 cm^2) were vertically placed into the solution. Afterward, the autoclave was heated to 140 °C and held at this temperature for 10 h. Subsequently, the obtained composite membranes were immersed in ethanol, followed by ultrasonic treatment for 5 min to remove excess COF powders. Then the membranes were thoroughly washed with mesitylene, tetrahydrofuran, and acetone, respectively. After cleaning, the membranes were dried under vacuum at 100 °C for 24 h. After solvothermal synthesis,

https://dx.doi.org/10.1021/acs.langmuir.0c02405
Langmuir 2020, 36, 12030−12037

the color of the CNTs membranes turned from black to metallic green, indicating that TpPa was coated on the membranes successfully. In order to achieve better carbonization of coated TpPa, the carbonization temperature was selected as 500, 600, and 700 °C according to the TG result (Figure S1). All samples were put into a tubular furnace and heated from room temperature to the desired temperature with a heating rate of 2 °C·min^{-1} under an argon atmosphere. Then the samples were kept under the desired temperature for 4 h. After carbonization, the samples turned black with a metallic luster. Corresponding samples are denoted as n/T NCMEs (n and T represent the concentration of Tp and the carbonization temperature, respectively).

The CDI performance of NCMEs was tested in a homemade system.[36] The testing module was assembled by Teflon caps, testing NCMEs, and a spacer. All components were separated by insulated nonwoven fabrics and sealed with rubber gaskets. The testing module was cut off for ∼30 min in the prepared salt solution before testing. A 40 mL amount of NaCl solution with a concentration of 150 mg·L^{-1} was used as the testing solution. The solution was transported by a peristaltic pump with a flow rate of 3.8 mL·min^{-1}. During the CDI processes, the conductivity probe (SevenCompact, Mettler Toledo S230-K) was placed in the storage tank to record the conductivity changes of the NaCl solution every 2 min. The relationship between the solution concentration (mg·L^{-1}) and the electrical conductivity (μS·cm^{-1}) was obtained through a standard solution calibration test (Figure S2). The electrosorption capacity (EC, mg·g^{-1}) of the electrode materials was calculated by the following equation

$$\mathrm{EC} = \frac{(C_0 - C_e)V}{m} \quad (1)$$

where C_0 and C_e (mg·L^{-1}) are the initial and final concentrations of the NaCl solution, respectively, V (L) represents the volume of the NaCl solution, and m (g) stands for the total mass of the two electrodes.

Characterization. The surface morphologies of the samples were characterized by a field-emission scanning electron microscope (FESEM, Hitachi, S-4800). To detect the surface hydrophilicity changes, static water contact angles (WCAs) were measured by a contact angle goniometer (Maist, Dropmeter A100). Each sample was probed for at least 5 positions, and the average value of WCAs was reported. The crystal structures of all samples were obtained by an X-ray diffractometer (XRD, Rigaku, MiniFlex 600) within the 2θ range from 10° to 80°. The XRD of TpPa powder was detected on a powder X-ray diffraction diffractometer (PXRD, Rigaku, Smart Lab TM 3KW) at room temperature with Cu Kα radiation. The scanning range was from 5° to 40° with a scanning rate of 0.02°·s^{-1}. The thermal stability of TpPa-coated membranes was analyzed by a thermogravimetric analyzer (TGA, NETZSCH, STA449F3). The temperature was raised from 10 to 800 °C with a heating rate of 10 °C·min^{-1}. The C, N, and O contents of functionalized membranes were analyzed by an X-ray photoelectron spectrometer (XPS, Thermo Fisher Scientific, K-alpha). The disorder degree of the carbon electrodes was characterized on a Raman spectrometer (Thermo Fisher Scientific, Dxr 2Xi) with a laser wavelength of 532 nm.

Electrochemical Measurements. Electrochemical measurement of the membrane electrodes was carried out on an electrochemical workstation (Shanghai Chenhua, CHI660E) in which a 1 M NaCl solution was used as the testing solution. The testing samples, platinum wire, and Ag/AgCl electrode were used as the working electrodes, counter electrode, and reference electrode, respectively. Cyclic voltammetry (CV) was performed at different scan rates within the potential from −0.8 to 0.4 V. Electrochemical impedance spectroscopy (EIS) was conducted from 1 to 100 000 Hz under the voltage of 5 mV.

RESULTS AND DISCUSSION

Surface Morphologies of Membrane Electrodes. The pristine CNTs membranes exhibit a black color in macroscopic appearance before functionalization (Figure 1a). After being coated with TpPa, the color of the CNTs membranes turns into a metallic green (Figure 1b). Finally, the obtained NCMEs revert to black with a metallic luster after carbonization (Figure 1c). The insets in Figure 1b and 1c show that the functionalization processes have little influence on the mechanical properties of TpPa-coated CNTs membranes and NCMEs. To further investigate the microstructure changes, all samples were characterized by FESEM. The pristine membranes are formed by uniform and interconnected fibrous CNTs which exhibit three-dimensional porous structures (Figure 1d). After being coated by TpPa (1 mmol Tp), the average diameter of the CNTs matrices is significantly increased from 19.6 to 63.6 nm; therefore, the piled pore diameter of the membranes is reduced sharply (Figure 1e). Moreover, the average diameter of TpPa-coated CNTs increases with increasing Tp concentration (Figure S3). Due to the high-temperature carbonization processes, the TpPa turns into N-doping carbons and the diameter of the NCME backbones shrinks from 63.6 to 31.5 nm (Figure 1f). After forming NCMEs, the mass of 1/600 NCMEs is 1.8 times heavier than that of pristine CNTs membranes. From a macroscopic viewpoint, the color variation is the external manifestation of these microstructure changes.

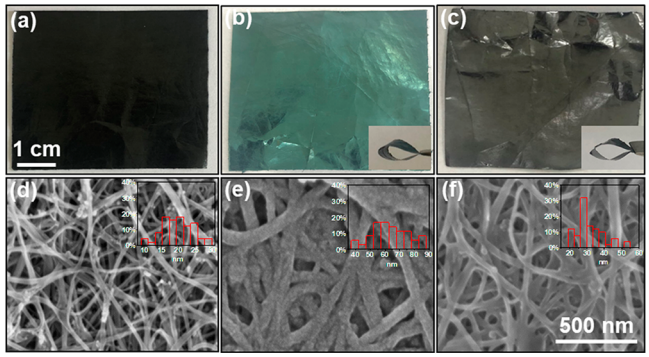

Figure 1. Photographs and SEM images of (a, d) pristine CNTs membranes, (b, e) TpPa-coated CNTs membranes, and (c, f) 1/600 NCMEs. (Insets in b and c) Manual bending images of corresponding samples. a−c have the same magnification, and scale bar is shown in a. d−f have the same magnification, and scale bar is shown in f. (Insets in d−f) Statistic results of the fibril diameter for each sample.

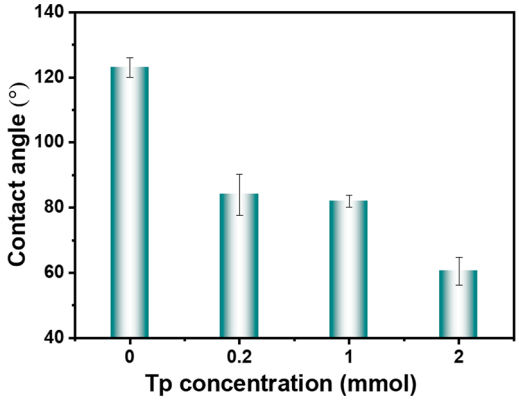

Figure 2. WCAs of NCMEs carbonized under 600 °C with different Tp concentrations.

Wettability and Surface Composition of Membrane Electrodes. The wettability of the electrodes determines the affinity between the electrodes and water, which plays a vital

https://dx.doi.org/10.1021/acs.langmuir.0c02405
Langmuir 2020, 36, 12030−12037

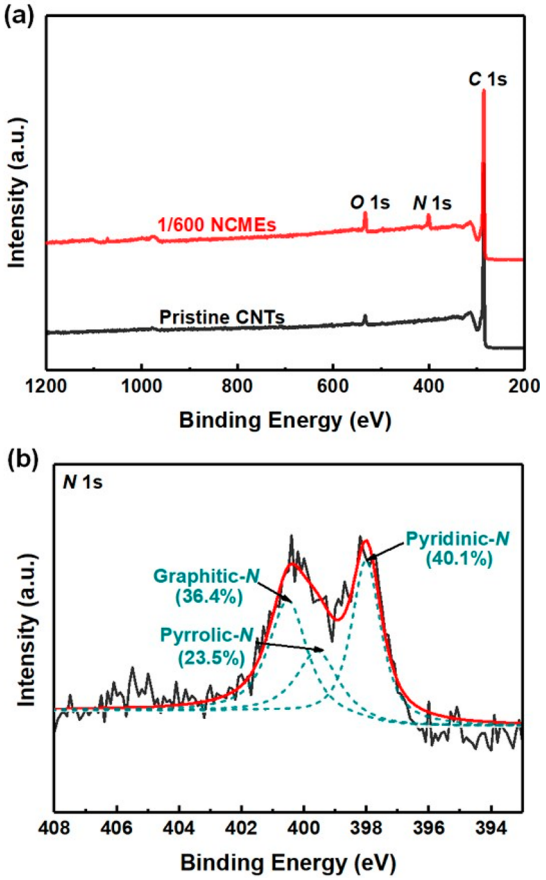

Figure 3. (a) XPS survey spectra of pristine CNTs membranes and 1/600 NCMEs. (b) High-resolution N 1s XPS spectrum of 1/600 NCMEs.

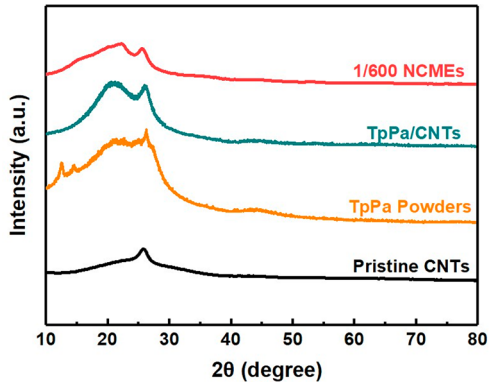

Figure 4. XRD patterns of TpPa powders, membranes, and 1/600 NCMEs.

role in the desalination processes. Due to the electron-rich property, the doping of N will enhance the hydrophilicity of the CNTs membranes electrodes.[37] To evaluate the wettability of the electrodes, WCAs of pristine CNTs membranes and NCMEs fabricated under different conditions were tested. As shown in Figure 2, the WCA of pristine CNT membranes is ~120°, which exhibits a strong hydrophobicity. After solvothermal growth and carbonization, the WCAs of all *n*/600 NCMEs are lower than 90°, which exhibit better hydrophilicity than the CNTs membranes. This result confirms that the doping of the N element can improve the wettability of NCMEs. We also examined the influence of the carbon-

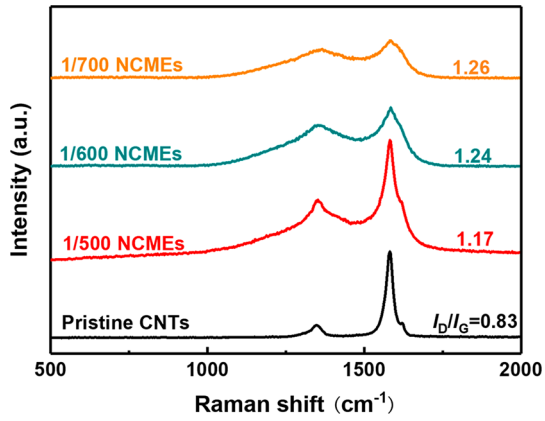

Figure 5. Raman spectra of pristine CNTs membranes and NCMEs carbonized at different temperatures.

ization temperatures on the wettability of the electrodes (Figure S4). Unfortunately, the NCMEs carbonized at lower (500 °C) or higher (700 °C) temperatures exhibit worse hydrophilicity than the 1/600 NCMEs. According to the TG result, the weight loss at 500 °C was less than that at 600 °C, which implies that the TpPa might be incompletely turned into N-doping porous carbons. In contrast, the samples carbonized at 700 °C faced significant loss of the N element. With a lower N content, the active sites on the electrode surface or pores were also decreased; thus, the affinity between the electrodes and water was weakened. Therefore, the NCMEs fabricated at 500 or 700 °C exhibited lower hydrophilicity.

To further investigate the influence of N doping on the chemical composition of NCMEs, we employ XPS to examine the element content changes. As shown in Figure 3a, the pristine CNTs membranes are primarily composed of the C element. The small amount of O on the membranes may derive from oxidation of CNTs, and there is no N element that can be found. Different from the pristine membranes, the 1/600 NCMEs exhibit an obvious N 1s peak, implying that the N element (~6.03% atomic ratio, Table S1) is successfully doped into CNTs membranes. To further analyze the chemical state of the N element in 1/600 NCMEs, the N 1s spectrum is interpreted carefully. As shown in Figure 3b, there are three forms of N element on the electrodes, namely, the graphitic-N (401.1 eV, 36.4%), the pyrrolic-N (399.6 eV, 23.5%), and the pyridinic-N (398.2 eV, 40.1%).[33] Graphitic-N can enhance the conductivity of electrode materials, while the pyridinic-N and pyrrolic-N can improve the capacitance properties of the electrode materials. These results demonstrate that the doped N element has the potential to improve the electrosorption and capacitance of CDI electrodes.[26,38]

Crystallinity of NCMEs. The crystallinity of the electrode materials will affect the lifetime of the charge carriers, which will further influence the deionization processes.[39] Therefore, we examine the influence of the fabrication parameters on the crystallinity of NCMEs. As shown in Figure S5a, the PXRD pattern of powders collected from the Teflon-lined autoclave confirmed that we synthesized TpPa successfully. According to the XRD patterns, every sample showed a peak around 26° (Figures 4 and S5b). For TpPa powders, this peak can be attributed to the $\pi-\pi$ stacking structure,[40] while for other samples this peak corresponded to the (002) plane of the CNTs (JCPDS No. 41-1487).[41] After being coated with TpPa, the TpPa/CNTs sample showed a peak at 21.5° which could

https://dx.doi.org/10.1021/acs.langmuir.0c02405
Langmuir 2020, 36, 12030−12037

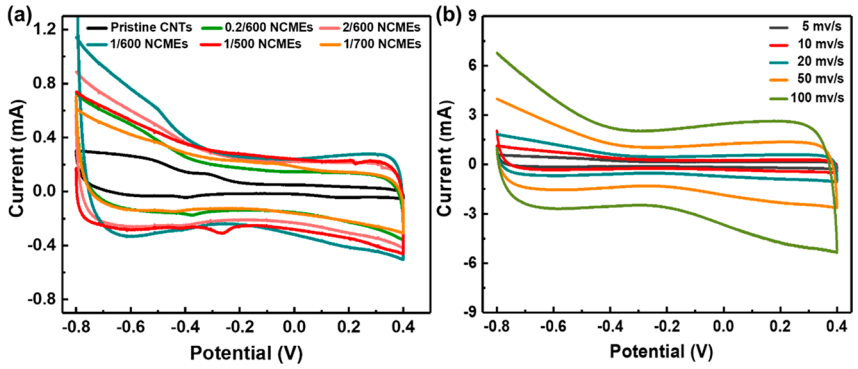

Figure 6. (a) CV curves of the pristine CNTs membranes and NCMEs at a scan rate of 10 mV·s^{-1}. (b) CV profiles of 1/600 NCMEs at different scan rates. All curves were obtained in 1 M NaCl solution.

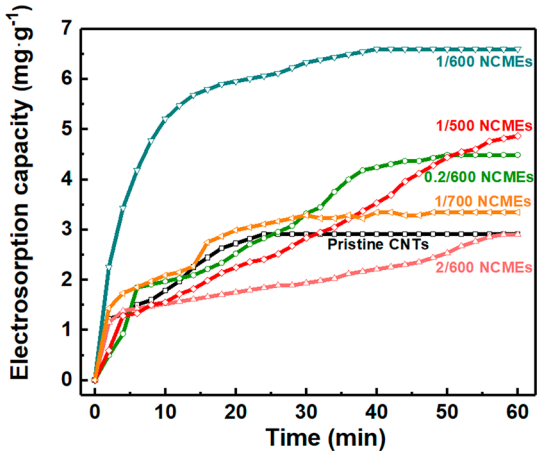

Figure 7. Electrosorption capacity of pristine CNTs membrane and NCMEs in 150 mg·L^{-1} NaCl solution.

be attributed to the successful coating of TpPa on CNTs membranes. Interestingly, the samples prepared with moderate conditions (lower precursor concentrations or carbonization temperatures) exhibit a peak in the range of 20−25° (0.2/600, 1/500, and 1/600 NCMEs), which is attributed to formation of the graphitic-N structure in the doped carbon.[34,42] This peak is gradually disappearing with intensified preparation conditions (2/600 and 1/700 NCMEs), which is caused by the incomplete reaction (2/600 NCMEs) or over reaction (1/700 NCMEs) of the coated TpPa. According to XRD spectra, the 1/600 NCMEs show the strongest peak within the range of 20−25°. As mentioned above, the graphitic structures in the electrodes facilitate the transfer of electrons; thus, the 1/600 NCMEs may have better electron transfer capability than other samples.

Raman is a common method to characterize the disorder degrees of carbon materials. In Figure 5, the peaks at 1350 and 1580 cm^{-1} correspond to the D and G bands of prepared NCMEs, respectively. The D band indicates the disordered carbon or graphitization defects in the NCMEs. The G band represents the sp^2 hybridization structure of the carbon materials. The relative intensity ratio of these two peaks (I_D/I_G) reflects the degree of graphitization or defect of the electrode materials. It is obvious that the I_D/I_G ratios of NCMEs are higher than that of the original CNTs membranes. The I_D/I_G ratios of CNTs, 1/500 NCMEs, 1/600 NCMEs, and 1/700 NCMEs are 0.83, 1.17, 1.24, and 1.26, respectively, which implies that the disorder degree of the NCMEs is

Table 1. Comparison of the Electrosorption Capacity of 1/600 NCMEs with Other Reported Electrodes

electrodes	applied voltage (V)	NaCl concentration (mg·L^{-1})	EC (mg·g^{-1})	ref
channel-structured graphene	1.5	295	9.6	18
MOGs	1.4	500	25.16	24
N-doped porous carbon tubes	1.2	500	16.7	33
CTF COFs	1.2	1000	29.34	35
CNT@20TiO$_2$	1.6	40	5.09	36
N-doped graphene sponge	1.2	500	4.5	38
COFs-derived porous carbon spheres	1.2	500	10.3	42
carbon nanotube sponge	1.2	60	4.3	46
hollow carbon nanofibers	1.2	45	1.9	47
porous carbon spheres	1.2	500	5.8	48
sponge-templated graphene	1.5	50	5.0	49
porous carbon nanofibers	1.2	500	8.1	50
N-doped hierarchical porous carbon	1.2	500	10.29	51
polyaniline-modified activated carbon	1.2	250	3.15	52
1/600 NCMEs	1.2	150	6.59	*This work*

increasing with higher carbonization temperatures. After doping, some C atoms in the NCMEs are replaced by N atoms; therefore, the structure defects of the carbon materials are increasing. For CDI processes, these newly formed defects are beneficial because they will act as active sites and accommodate more ions.[43] Combining the XRD and Raman results, we assume that the 1/600 NCMEs will manifest better CDI performance than other samples.

Electrochemical Performance of NCMEs. The electrochemical measurement is an effective way to evaluate the electrochemical properties of electrode materials. The CV curves of NCMEs fabricated with different conditions are shown in Figure 6a. All NCMEs were tested under a potential from −0.8 to 0.4 V with a scan rate of 10 mv·s^{-1}. Comparing with other curves, the CV profile of 1/600 NCMEs shows a nearly rectangular shape, which is a typical electrical double-layer (EDL) capacitive behavior. Moreover, the CV profile of 1/600 NCMEs also exhibits the largest encircled area,

https://dx.doi.org/10.1021/acs.langmuir.0c02405
Langmuir 2020, 36, 12030−12037

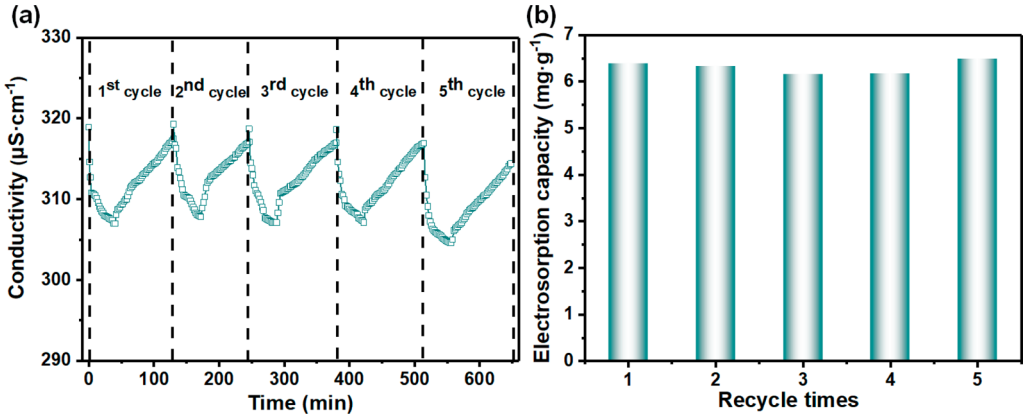

Figure 8. (a) Deionization-regeneration curves. (b) Electrosorption capacities of the 1/600 NCMEs.

indicating that the pores of 1/600 NCMEs provide better ion diffusion and confirms the NCMEs fabricated under such condition have the best capacitance. The 1/600 NCMEs were also tested with different scanning rates (from 2 to 100 mv·s^{-1}). As shown in Figure 6b, the CV curves have a good rectangular shape at low scanning rates, which means that the ions in solution can enter and exit the pores quickly. Therefore, the total surface of the electrode can be utilized better. However, when the scanning rates are higher than 20 mV·s^{-1}, formation of capacitance is delayed by higher currents, indicating the sodium and chloride ions in solution do not have enough time to enter the electrode pores; thus, the ideal EDL capacitance effect cannot be formed.[44,45] Importantly, the 1/600 NCMEs have the lowest impedance (Figure S6), which can lead to rapid transfer of charge. Combining these results, we can conclude that the 1/600 NCMEs exhibit better electrochemical performance than other NCMEs.

CDI Performance of NCMEs. CDI desalinization testing of all NCMEs was performed in a 150 mg·L^{-1} NaCl solution under a constant voltage of 1.2 V. As shown in Figure 7, the 1/600 NCMEs are the best EC. All samples exhibit a quick adsorption rate at the initial stage, but most of the quick adsorption stages are less than 4 min. It is worth noting that the 1/600 NCMEs kept the fast adsorption rate for more than 10 min; then the rate slows down, and the adsorption amount reaches equilibrium after 40 min. After being doped with only 6.03% N element, the EC of 1/600 NCMEs reaches 6.59 mg·g^{-1}, which is ∼2.3 times higher than that of the pristine CNTs membranes (2.91 mg·g^{-1}). As mentioned above, the graphitic-N in carbon materials will enhance the transfer of electrons and accommodate more ions, both of which are influential factors for CDI processes. Therefore, the CDI performance of NCMEs will change with the status of the graphitic-N structure. As illustrated by XRD characterization, the intensity of the graphitic-N peak increased first and then decreased with the ascending Tp concentrations or carbonization temperatures. Therefore, the EC of NCMEs fabricated with different Tp concentrations or carbonization temperatures kept in pace with the changing trend of graphitic-N content.

Comparing with CDI electrodes fabricated by other methods, the NCMEs show good electrosorption capacity (Table 1). Moreover, this proof-of-concept strategy exhibits some merits not shared by other preparation methods. First, the integration fabrication method avoids agglomeration usually faced using powder materials; thus, the structures of CNTs membranes and N-doping carbons are well preserved. Second, no extra additives are required to add in the electrodes; therefore, the risk of pore blocking during the fabrication process is averted. Third, the preparation processes are highly controllable; the morphology and composition of the prepared NCMEs can be regulated by changing the Tp concentration.

Regeneration and Reusability of NCMEs. CDI is an application-oriented desalination technology; therefore, the reusability of electrodes plays a key role in the application of CDI. To evaluate the reusability of NCMEs, repetitive electrosorption−desorption experiments were conducted on the 1/600 NCMEs. Adsorption and regeneration experiments were conducted under 1.2 and 0 V in 150 mg·L^{-1} NaCl solution several times. As shown in Figure 8a, the electrosorption procedure is completed within 40 min, which is consistent with the CDI testing result. Although the desorption time of NCMEs is prolonged slightly after being reused several times, the conductivity of the NaCl solution shows no obvious decrease, indicating that NCMEs have superior electrosorption−desorption performance after charging and discharging five times. Moreover, the 1/600 NCMEs show stable EC during the test (Figure 8b), which further confirms its good reusability for practical applications.

CONCLUSION

In this work, we propose an integrated strategy to turn the COF-coated CNTs membranes into high-performance NCMEs, which avoids the cumbersome forming processes facing conventional electrode fabrications. We demonstrate that COFs can be easily grown on the CNTs membranes using solvothermal growth and used as precursor to construct nitrogen-containing graphitic, pyridinic, and pyrrolic structures in porous carbon materials after carbonization. The wettability and electrosorption capacity of NCMEs are promoted significantly after doping only 6.03% N element. The 1/600 NCMEs exhibit ∼2.3 times higher electrosorption capacity than pristine CNTs membranes, and the NCMEs can be reused several times without performance degradation. These results confirm that COFs not only can be used as excellent carbon source to fabricate high-performance NCMEs for CDI but also are additions to the rapidly expanding field of carbon materials electrochemistry.

https://dx.doi.org/10.1021/acs.langmuir.0c02405
Langmuir 2020, 36, 12030−12037

■ ASSOCIATED CONTENT

Supporting Information

The Supporting Information is available free of charge at https://pubs.acs.org/doi/10.1021/acs.langmuir.0c02405.

TGA of TpPa-coated CNTs membranes; calibration of NaCl solution; SEM images; WCAs of NCMEs; PXRD and XRD patterns; elemental content analysis; EIS of different NCMEs (PDF)

■ AUTHOR INFORMATION

Corresponding Authors

Sen Xiong − *State Key Laboratory of Materials-Oriented Chemical Engineering, College of Chemical Engineering, Nanjing Tech University, Nanjing, Jiangsu 211816, P. R. China*; Email: xiongsenhg@njtech.edu.cn

Yong Wang − *State Key Laboratory of Materials-Oriented Chemical Engineering, College of Chemical Engineering, Nanjing Tech University, Nanjing, Jiangsu 211816, P. R. China*; orcid.org/0000-0002-8653-514X; Email: yongwang@njtech.edu.cn

Authors

Li Ren − *State Key Laboratory of Materials-Oriented Chemical Engineering, College of Chemical Engineering, Nanjing Tech University, Nanjing, Jiangsu 211816, P. R. China*

Jiemei Zhou − *State Key Laboratory of Materials-Oriented Chemical Engineering, College of Chemical Engineering, Nanjing Tech University, Nanjing, Jiangsu 211816, P. R. China*

Complete contact information is available at: https://pubs.acs.org/10.1021/acs.langmuir.0c02405

Notes

The authors declare no competing financial interest.

■ ACKNOWLEDGMENTS

We gratefully acknowledge financial support from the National Key Research and Development Program of China (2018YFE0203502), Jiangsu Natural Science Foundation (BK20190677), and Program of Excellent Innovation Teams of Jiangsu Higher Education Institutions.

■ REFERENCES

(1) Oren, Y. Capacitive Delonization (CDI) for Desalination and Water Treatment - Past, Present and Future (A Review). *Desalination* **2008**, *228*, 10−29.

(2) Porada, S.; Zhao, R.; van der Wal, A.; Presser, V.; Biesheuvel, P. M. Review on the Science and Technology of Water Desalination by Capacitive Deionization. *Prog. Mater. Sci.* **2013**, *58*, 1388−1442.

(3) Suss, M. E.; Porada, S.; Sun, X.; Biesheuvel, P. M.; Yoon, J.; Presser, V. Water Desalination via Capacitive Deionization: What Is It and What Can We Expect from It? *Energy Environ. Sci.* **2015**, *8*, 2296−2319.

(4) Sufiani, O.; Elisadiki, J.; Machunda, R. L.; Jande, Y. A. C. Modification Strategies to Enhance Electrosorption Performance of Activated Carbon Electrodes for Capacitive Deionization Applications. *J. Electroanal. Chem.* **2019**, *848*, 113328.

(5) Lv, H. H.; Wang, Y.; Wu, L. Y.; Hu, Y. D. Numerical Simulation and Optimization of the Flash Chamber for Multi-Stage Flash Seawater Desalination. *Desalination* **2019**, *465*, 69−78.

(6) Qin, M. H.; Deshmukh, A.; Epsztein, R.; Patel, S. K.; Owoseni, O. M.; Walker, W. S.; Elimelech, M. Comparison of Energy Consumption in Desalination by Capacitive Deionization and Reverse Osmosis. *Desalination* **2019**, *455*, 100−114.

(7) Anderson, M. A.; Cudero, A. L.; Palma, J. Capacitive Deionization as an Electrochemical Means of Saving Energy and Delivering Clean Water. Comparison to Present Desalination Practices: Will It Compete? *Electrochim. Acta* **2010**, *55*, 3845−3856.

(8) Ahmed, M. A.; Tewari, S. Capacitive Deionization: Processes, Materials and State of the Technology. *J. Electroanal. Chem.* **2018**, *813*, 178−192.

(9) Liu, N. L.; Chen, L. I.; Tsai, S. W.; Hou, C. H. Enhanced Desalination of Electrospun Activated Carbon Fibers with Controlled Pore Structures in the Electrosorption Process. *Environ. Sci.-Wat. Res. Technol.* **2020**, *6*, 312−320.

(10) Sebti, E.; Besli, M. M.; Metzger, M.; Hellstrom, S.; Schultz-Neu, M. J.; Alvarado, J.; Christensen, J.; Doeff, M.; Kuppan, S.; Subban, C. V. Removal of Na^+ and Ca^{2+} with Prussian Blue Analogue Electrodes for Brackish Water Desalination. *Desalination* **2020**, *487*, 114479.

(11) Cuong, D. V.; Wu, P.-C.; Liu, N.-L.; Hou, C.-H. Hierarchical Porous Carbon Derived From Activated Biochar as an Eco-Friendly Electrode for the Electrosorption of Inorganic Ions. *Sep. Purif. Technol.* **2020**, *242*, 116813.

(12) Leong, Z. Y.; Yang, H. Y. Capacitive Deionization of Divalent Cations for Water Softening Using Functionalized Carbon Electrodes. *ACS Omega* **2020**, *5*, 2097−2106.

(13) Kyaw, H. H.; Myint, M. T. Z.; Al-Harthi, S.; Al-Abri, M. Removal of Heavy Metal Ions by Capacitive Deionization: Effect of Surface Modification on Ions Adsorption. *J. Hazard. Mater.* **2020**, *385*, 121565.

(14) Kalfa, A.; Shapira, B.; Shopin, A.; Cohen, I.; Avraham, E.; Aurbach, D. Capacitive Deionization for Wastewater Treatment: Opportunities and Challenges. *Chemosphere* **2020**, *241*, 125003.

(15) Kumar, R.; Sen Gupta, S.; Katiyar, S.; Raman, V. K.; Varigala, S. K.; Pradeep, T.; Sharma, A. Carbon Aerogels through Organo-Inorganic Co-Assembly and Their Application in Water Desalination by Capacitive Deionization. *Carbon* **2016**, *99*, 375−383.

(16) Liu, Y. H.; Hsi, H. C.; Li, K. C.; Hou, C. H. Electrodeposited Manganese Dioxide/Activated Carbon Composite as a High-Performance Electrode Material for Capacitive Deionization. *ACS Sustainable Chem. Eng.* **2016**, *4*, 4762−4770.

(17) Wang, H.; Zhang, D. S.; Yan, T. T.; Wen, X. R.; Zhang, J. P.; Shi, L. Y.; Zhong, Q. D. Three-Dimensional Macroporous Graphene Architectures as High Performance Electrodes for Capacitive Deionization. *J. Mater. Chem. A* **2013**, *1*, 11778−11789.

(18) Chang, L.; Hang Hu, Y. 3D Channel-Structured Graphene as Efficient Electrodes for Capacitive Deionization. *J. Colloid Interface Sci.* **2019**, *538*, 420−425.

(19) Zhang, D. S.; Yan, T. T.; Shi, L. Y.; Peng, Z.; Wen, X. R.; Zhang, J. P. Enhanced Capacitive Deionization Performance of Graphene/Carbon Nanotube Composites. *J. Mater. Chem.* **2012**, *22*, 14696−14704.

(20) Xie, Z.; Shang, X.; Yan, J.; Hussain, T.; Nie, P.; Liu, J. Biomass-Derived Porous Carbon Anode for High-Performance Capacitive Deionization. *Electrochim. Acta* **2018**, *290*, 666−675.

(21) Tu, Y. H.; Liu, C. F.; Wang, J. A.; Hu, C. C. Construction of an Inverted-Capacitive Deionization System Utilizing Pseudocapacitive Materials. *Electrochem. Commun.* **2019**, *104*, 106486.

(22) Chang, L.; Li, J.; Duan, X.; Liu, W. Porous Carbon Derived From Metal-Organic Framework (MOF) for Capacitive Deionization Electrode. *Electrochim. Acta* **2015**, *176*, 956−964.

(23) Xie, J. Z.; Ma, J. X.; Wu, L. L.; Xu, M.; Ni, W.; Yan, Y. M. Carbon Nanotubes in-Situ Cross-Linking the Activated Carbon Electrode for High-Performance Capacitive Deionization. *Sep. Purif. Technol.* **2020**, *239*, 116593.

(24) Wang, Z.; Yan, T.; Chen, G.; Shi, L.; Zhang, D. High Salt Removal Capacity of Metal-Organic Gel Derived Porous Carbon for Capacitive Deionization. *ACS Sustainable Chem. Eng.* **2017**, *5*, 11637−11644.

(25) Hsu, C. C.; Tu, Y. H.; Yang, Y. H.; Wang, J. A.; Hu, C. C. Improved Performance and Long-Term Stability of Activated Carbon

Doped with Nitrogen for Capacitive Deionization. *Desalination* **2020**, *481*, 114362.
(26) Xu, X.; Allah, A. E.; Wang, C.; Tan, H.; Farghali, A. A.; Khedr, M. H.; Malgras, V.; Yang, T.; Yamauchi, Y. Capacitive Deionization Using Nitrogen-Doped Mesostructured Carbons for Highly Efficient Brackish Water Desalination. *Chem. Eng. J.* **2019**, *362*, 887−896.
(27) Xu, F.; Jin, S.; Zhong, H.; Wu, D.; Yang, X.; Chen, X.; Wei, H.; Fu, R.; Jiang, D. Electrochemically Active, Crystalline, Mesoporous Covalent Organic Frameworks on Carbon Nanotubes for Synergistic Lithium-Ion Battery Energy Storage. *Sci. Rep.* **2015**, *5*, 8225.
(28) Li, H.; Chang, J. H.; Li, S. S.; Guan, X. Y.; Li, D. H.; Li, C. Y.; Tang, L. X.; Xue, M.; Yan, Y. S.; Valtchev, V.; Qiu, S. L.; Fang, Q. R. Three-Dimensional Tetrathiafulvalene-Based Covalent Organic Frameworks for Tunable Electrical Conductivity. *J. Am. Chem. Soc.* **2019**, *141*, 13324−13329.
(29) Zhang, K.; Kirlikovali, K. O.; Varma, R. S.; Jin, Z.; Jang, H. W.; Farha, O. K.; Shokouhimehr, M. Covalent Organic Frameworks: Emerging Organic Solid Materials for Energy and Electrochemical Applications. *ACS Appl. Mater. Interfaces* **2020**, *12*, 27821−27852.
(30) Xiao, A.; Zhang, Z.; Shi, X.; Wang, Y. Enabling Covalent Organic Framework Nanofilms for Molecular Separation: Perforated Polymer-Assisted Transfer. *ACS Appl. Mater. Interfaces* **2019**, *11*, 44783−44791.
(31) Zhang, Z.; Shi, X.; Wang, R.; Xiao, A.; Wang, Y. Ultra-Permeable Polyamide Membranes Harvested by Covalent Organic Framework Nanofiber Scaffolds: A Two-in-One Strategy. *Chem. Sci.* **2019**, *10*, 9077−9083.
(32) Ding, X. S.; Guo, J.; Feng, X. A.; Honsho, Y.; Guo, J. D.; Seki, S.; Maitarad, P.; Saeki, A.; Nagase, S.; Jiang, D. L. Synthesis of Metallophthalocyanine Covalent Organic Frameworks that Exhibit High Carrier Mobility and Photoconductivity. *Angew. Chem., Int. Ed.* **2011**, *50*, 1289−1293.
(33) Zhao, Y.; Luo, G.; Zhang, L.; Gao, L.; Zhang, D.; Fan, Z. Nitrogen-Doped Porous Carbon Tubes Composites Derived from Metal-Organic Framework for Highly Efficient Capacitive Deionization. *Electrochim. Acta* **2020**, *331*, 135420.
(34) Zhang, X.; Zhu, G.; Wang, M.; Li, J.; Lu, T.; Pan, L. Covalent-Organic-Frameworks Derived N-Doped Porous Carbon Materials as Anode for Superior Long-Life Cycling Lithium and Sodium Ion Batteries. *Carbon* **2017**, *116*, 686−694.
(35) Liu, D.; Ning, X.-a.; Hong, Y.; Li, Y.; Bian, Q.; Zhang, J. Covalent Triazine-Based Frameworks as Electrodes for High-Performance Membrane Capacitive Deionization. *Electrochim. Acta* **2019**, *296*, 327−334.
(36) Feng, J.; Xiong, S.; Wang, Y. Atomic Layer Deposition of TiO_2 on Carbon-Nanotube Membranes for Enhanced Capacitive Deionization. *Sep. Purif. Technol.* **2019**, *213*, 70−77.
(37) Li, J.; Han, K.; Wang, D.; Teng, Z.; Cao, Y.; Qi, J.; Li, M.; Wang, M. Fabrication of High Performance Structural N-Doped Hierarchical Porous Carbon for Supercapacitor. *Carbon* **2020**, *164*, 42−50.
(38) Xu, X.; Sun, Z.; Chua, D. H. C.; Pan, L. Novel Nitrogen Doped Graphene Sponge with Ultrahigh Capacitive Deionization Performance. *Sci. Rep.* **2015**, *5*, 11225.
(39) Wang, S.; Sun, Q.; Chen, W.; Tang, Y.; Aguila, B.; Pan, Y.; Zheng, A.; Yang, Z.; Wojtas, L.; Ma, S.; Xiao, F.-S. Programming Covalent Organic Frameworks for Photocatalysis: Investigation of Chemical and Structural Variations. *Matter* **2020**, *2*, 416−427.
(40) Kandambeth, S.; Mallick, A.; Lukose, B.; Mane, M. V.; Heine, T.; Banerjee, R. Construction of Crystalline 2D Covalent Organic Frameworks with Remarkable Chemical (Acid/Base) Stability via a Combined Reversible and Irreversible Route. *J. Am. Chem. Soc.* **2012**, *134*, 19524−19527.
(41) Zhu, X.; Xia, Y.; Zhang, X.; Al-Khalaf, A. A.; Zhao, T.; Xu, J.; Peng, L.; Hozzein, W. N.; Li, W.; Zhao, D. Synthesis of Carbon Nanotubes@Mesoporous Carbon Core-Shell Structured Electrocatalysts via a Molecule-Mediated Interfacial Co-Assembly Strategy. *J. Mater. Chem. A* **2019**, *7*, 8975−8983.
(42) Li, Y.; Xu, X.; Hou, S.; Ma, J.; Lu, T.; Wang, J.; Yao, Y.; Pan, L. Facile Dual Doping Strategy via Carbonization of Covalent Organic Frameworks to Prepare Hierarchically Porous Carbon Spheres for Membrane Capacitive Deionization. *Chem. Commun.* **2018**, *54*, 14009−14012.
(43) Liu, Y.; Xu, X.; Wang, M.; Lu, T.; Sun, Z.; Pan, L. Metal-Organic Framework-Derived Porous Carbon Polyhedra for Highly Efficient Capacitive Deionization. *Chem. Commun.* **2015**, *51*, 12020−12023.
(44) Liu, H. Y.; Wang, K. P.; Teng, H. S. A Simplified Preparation of Mesoporous Carbon and the Examination of the Carbon Accessibility for Electric Double Layer Formation. *Carbon* **2005**, *43*, 559−566.
(45) Wen, X.; Zhang, D.; Yan, T.; Zhang, J.; Shi, L. Three-dimensional graphene-based hierarchically porous carbon composites prepared by a dual-template strategy for capacitive deionization. *J. Mater. Chem. A* **2013**, *1*, 12334−12344.
(46) Wang, L.; Wang, M.; Huang, Z.-H.; Cui, T.; Gui, X.; Kang, F.; Wang, K.; Wu, D. Capacitive Deionization of Nacl Solutions Using Carbon Nanotube Sponge Electrodes. *J. Mater. Chem.* **2011**, *21*, 18295−18299.
(47) El-Deen, A. G.; Barakat, N. A. M.; Khalil, K. A.; Kim, H. Y. Hollow Carbon Nanofibers as an Effective Electrode for Brackish Water Desalination Using the Capacitive Deionization Process. *New J. Chem.* **2014**, *38*, 198−205.
(48) Liu, Y.; Pan, L.; Chen, T.; Xu, X.; Lu, T.; Sun, Z.; Chua, D. H. C. Porous Carbon Spheres via Microwave-Assisted Synthesis for Capacitive Deionization. *Electrochim. Acta* **2015**, *151*, 489−496.
(49) Yang, Z.-Y.; Jin, L.-J.; Lu, G.-Q.; Xiao, Q.-Q.; Zhang, Y.-X.; Jing, L.; Zhang, X.-X.; Yan, Y.-M.; Sun, K.-N. Sponge-Templated Preparation of High Surface Area Graphene with Ultrahigh Capacitive Deionization Performance. *Adv. Funct. Mater.* **2014**, *24*, 3917−3925.
(50) Pan, H.; Yang, J.; Wang, S.; Xiong, Z.; Cai, W.; Liu, J. Facile Fabrication of Porous Carbon Nanofibers by Electrospun PAN/Dimethyl Sulfone for Capacitive Deionization. *J. Mater. Chem. A* **2015**, *3*, 13827−13834.
(51) Li, Y.; Hussain, I.; Qi, J.; Liu, C.; Li, J.; Shen, J.; Sun, X.; Han, W.; Wang, L. N-Doped Hierarchical Porous Carbon Derived from Hypercrosslinked Diblock Copolymer for Capacitive Deionization. *Sep. Purif. Technol.* **2016**, *165*, 190−198.
(52) Yan, C. J.; Zou, L. D.; Short, R. Polyaniline-Modified Activated Carbon Electrodes for Capacitive Deionisation. *Desalination* **2014**, *333*, 101−106.

https://dx.doi.org/10.1021/acs.langmuir.0c02405
Langmuir 2020, 36, 12030−12037